Approaches towards long-pulse divertor operations on EAST by active control of plasma–wall interactions

2014 Nucl. Fusion 54 013002

(http://iopscience.iop.org/0029-5515/54/1/013002)

IOP Publishing | International Atomic Energy Agency Nuclear Fusion
Nucl. Fusion **54** (2014) 013002 (9pp) doi:10.1088/0029-5515/54/1/013002

Approaches towards long-pulse divertor operations on EAST by active control of plasma–wall interactions

H.Y. Guo[1,2], J. Li[1], X.Z. Gong[1], B.N. Wan[1], J.S. Hu[1], L. Wang[1], H.Q. Wang[1], J.E. Menard[3], M.A. Jaworski[3], K.F. Gan[1], S.C. Liu[1], G.S. Xu[1], S.Y. Ding[1], L.Q. Hu[1], Y.F. Liang[4], J.B. Liu[1], G.N. Luo[1], H. Si[1], D.S. Wang[1], Z.W. Wu[1], L.Y. Xiang[1], B.J. Xiao[1], L. Zhang[1], X.L. Zou[5], D.L. Hillis[6], A. Loarte[7], R. Maingi[3,6] and the EAST Team[1]

[1] Institute of Plasma Physics, Chinese Academy of Sciences, Hefei 230031, People's Republic of China
[2] Tri Alpha Energy, PO Box 7010, Rancho Santa Margarita, CA 92610, USA
[3] Princeton Plasma Physics Laboratory, PO Box 451, Princeton, NJ 08543, USA
[4] Forschungszentrum Jülich GmbH, Association EURATOM-FZ Jülich, Institut für Energie-und Klimaforschung-Plasmaphysik, Trilateral Euregio Cluster, D-52425 Jülich, Germany
[5] CEA, IRFM, F-13108 Saint-Paul-lez-Durance, France
[6] Oak Ridge National Laboratory, Oak Ridge, TN 37831, USA
[7] ITER Organization, Route de Vinon sur Verdon, 13115 St Paul Lez Durance, France

E-mail: hyguo@ipp.ac.cn

Received 31 December 2012, accepted for publication 1 November 2013
Published 28 November 2013

Abstract

The Experimental Advanced Superconducting Tokamak (EAST) has demonstrated, for the first time, long-pulse divertor plasmas over 400 s, entirely driven by lower hybrid current drive (LHCD), and further extended high-confinement plasmas, i.e. H-modes, over 30 s with predominantly LHCD and advanced lithium wall conditioning. Many new and exciting physics results have been obtained in the quest for long-pulse operations. The key findings are as follows: (1) access to H-modes in EAST favours the divertor configuration with the ion ∇B drift directed away from the dominant X-point; (2) divertor asymmetry during edge-localized modes (ELMs) also appears to be dependent on the toroidal field direction, with preferential particle flow opposite to the ion ∇B drift; (3) LHCD induces a striated heat flux (SHF), enhancing heat deposition away from the strike point, and the degree of SHF can be modified by supersonic molecule beam injection; (4) the long-pulse H-modes in EAST exhibit a confinement quality between type-I and type-III ELMy H-modes, with $H_{98(y,2)} \sim 0.9$, similar to type-II ELMy H-modes.

Keywords: Tokamaks, power exhaust, divertors, plasma–material interactions, boundary layer effects

(Some figures may appear in colour only in the online journal)

1. Introduction

The Experimental Advanced Superconducting Tokamak (EAST) was built to demonstrate high-power, long-pulse operations under fusion-relevant conditions, with major radius $R = 1.9$ m, minor radius $a = 0.5$ m and envisioned pulse length up to 1000 s [1–3]. All of the magnetic coils, including 16 toroidal field coils, 6 poloidal field coils and 6 central solenoid coils, are superconductors made from niobium–titanium alloy embedded in copper. The maximum plasma current and toroidal field currently achieved in EAST are $I_p = 1$ MA and $B_T = 3.5$ T, which can be further increased to $I_p = 1.5$ MA and $B_T = 4$ T with the temperature of the superconducting magnets reduced from 4.5 to ~3.8 K.

EAST has an ITER-like D-shaped cross section with two symmetric divertors at the top and bottom, accommodating both single null (SN) and double null (DN) divertor configurations, as shown in figure 1. This, coupled with a flexible poloidal field control system, enables switching between various divertor configurations, i.e. lower single null (LSN), upper single null (USN) and DN during the same discharge, which significantly facilitates long-pulse operations, and provides a convenient tool for investigating divertor configuration effects, e.g. on divertor asymmetry, H-mode access, etc [4, 5]. The divertor geometry has adopted ITER-like vertical target structures with tightly fitted side baffles and a central dome in the private flux region to physically separate the inboard and outboard divertor

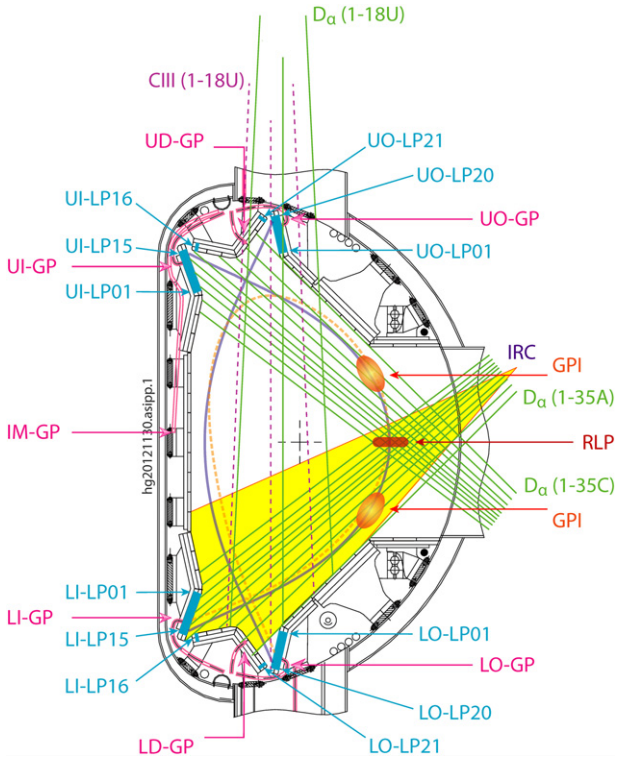

Figure 1. Poloidal cross section of EAST showing key divertor/edge diagnostics and divertor gas puff locations. C III—line emission of C^{2+} ions; D_α—Balmer-alpha emission of deuterium; GP—gas puff inlet; GPI—gas puff imaging; IM–inner midplane; IRC: infrared camera; LO(I)—lower outboard (inboard) divertor; LP—Langmuir probe; RLP—reciprocating Langmuir probe; U(L)D—upper (lower) divertor dome; UO(I)—upper outboard (inboard) divertor.

chambers, and to minimize the leakage of neutrals to the main chamber [4]. In addition, EAST has ITER-like heating schemes, i.e. dominated by electron heating from lower hybrid current drive (LHCD) and ion cyclotron resonance heating (ICRH), with actively water-cooled plasma-facing components (PFCs), thus providing a unique platform to address plasma physics and technology issues for ITER under steady-state operation conditions.

EAST will be one of the world's first magnetic confinement devices that must address plasma–wall interaction (PWI) issues facing high-power steady-state operations, which will ultimately limit its performance and operating space. Thus, it is essential to simultaneously control edge neutral recycling, impurity contamination and heat load on PFCs, especially on divertor target plates [6, 7]. In order to facilitate long-pulse operations, EAST has undertaken an extensive upgrade during the last shutdown to replace carbon tiles on the main chamber wall and divertor surface by molybdenum (Mo) tiles, except for those near the strike points, with enhanced baking capability over 250 °C. In addition, the following major means have been applied to EAST to actively control PWI.

- Active water cooling of all PFCs, allowing for steady-state operations with the maximum heat flux at 2 MW m^{-2}.
- Divertor pumping with a large internal toroidal cryopump, which is located under the outer divertor target at the bottom of the machine, with a pumping speed of 76 m^3 s^{-1} for D_2 and 107 m^3 s^{-1} for hydrogen to facilitate density control and particle exhaust.
- Advanced wall conditioning with lithium (Li) evaporation and real-time, *in situ* Li powder injection. The Li evaporation system has been newly upgraded to improve coating uniformity. This, along with enhanced wall baking capability and active water cooling, significantly facilitates recycling control.
- Active feedback control of divertor configurations, which allows the reliable control and change of magnetic configurations with strike point sweeping during a single discharge [8] to facilitate power exhaust and accommodate heating and current drive needs.
- Localized divertor gas puffing at various divertor locations, i.e. at the inner divertor, outer divertor and through the private flux region, for the control of peak heat fluxes and in–out divertor plasma asymmetries (figure 1).
- Furthermore, a new supersonic molecule beam injection (SMBI) system [9] has been implemented for the density maintenance and control of edge-localized modes (ELMs), in collaboration with the Southwestern Institute of Physics (SWIP), China.

With these augmented capabilities and control tools, EAST has recently demonstrated long-pulse divertor operations over 400 s, fully driven by LHCD, and further extended the high-confinement plasmas, i.e. H-modes, over 30 s [10]. This paper presents the recent progress on divertor physics studies for long-pulse operations in EAST, and is organized as follows. Section 2 describes the results on edge recycling control with Li wall conditioning. Section 3 contains new and rather intriguing results on the effects of divertor magnetic configuration on H-mode access and divertor asymmetry during ELMs in EAST. Section 4 describes the observation of LHCD-induced striated heat flux (SHF) at the divertor target and synergistic effects from SMBI, as well as heat flux control using conventional radiative divertor plasmas by argon (Ar) injection. Progress on long-pulse operations is demonstrated in section 5, which exhibits many desirable features for long-pulse H-mode maintenance with a dramatic reduction in transient power loads and good confinement quality. The summary and conclusions follow in section 6.

2. Recycling control and density maintenance

To facilitate density control and reduce edge recycling for long-pulse operations, extensive efforts have been made in developing wall conditioning techniques suitable for superconducting tokamaks, such as ion cyclotron resonant frequency (ICRF) wave-assisted wall conditioning and high-frequency glow discharge cleaning. In particular, we have explored various Li coating techniques. In addition to conventional Li evaporation, we have developed an advanced Li wall conditioning technique by coupling Li evaporation into ICRF plasma discharges [11, 12] to improve the uniformity of Li coverage on the wall in the presence of toroidal magnetic fields, which is unavoidable for a superconducting tokamak. Li wall conditioning has proven to be the most effective method employed in EAST to reduce not only impurities, but also neutral recycling and H content in deuterium plasmas

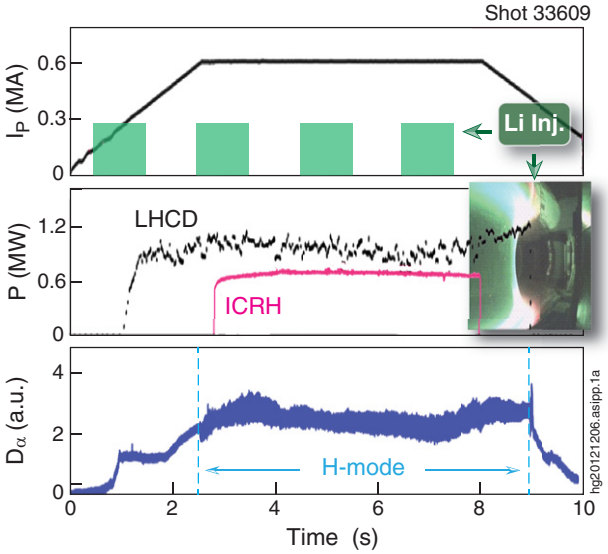

Figure 2. Longest H-mode achieved in EAST in the 2010 experimental campaign with real-time Li wall conditioning by the injection of Li powder from the top of the machine. Li radiation is seen by a charge-coupled device (CCD) camera as green light emissions in the divertor and edge plasmas, as shown in the inset.

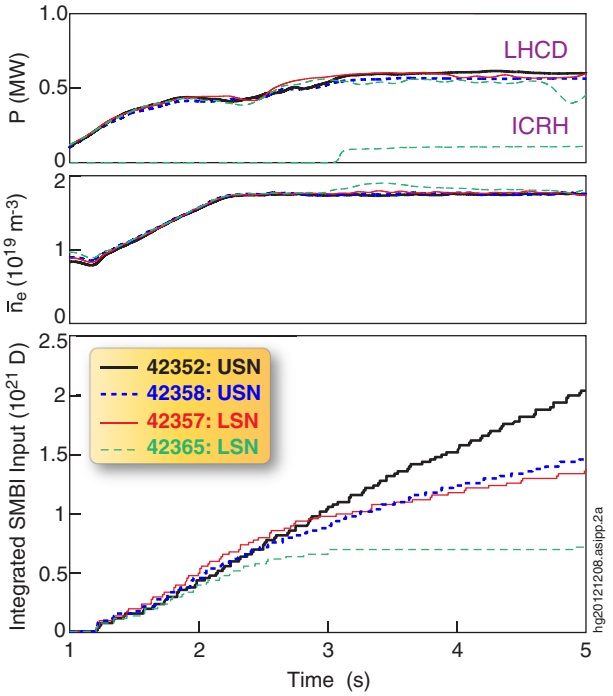

Figure 3. Time traces of auxiliary heating power from LHCD and ICRH, line-averaged electron density, $\bar{n}_e$, and integrated SMBI gas fuelling needed to maintain the requested density for a series of discharges, which followed the fresh Li coating (shot 42352).

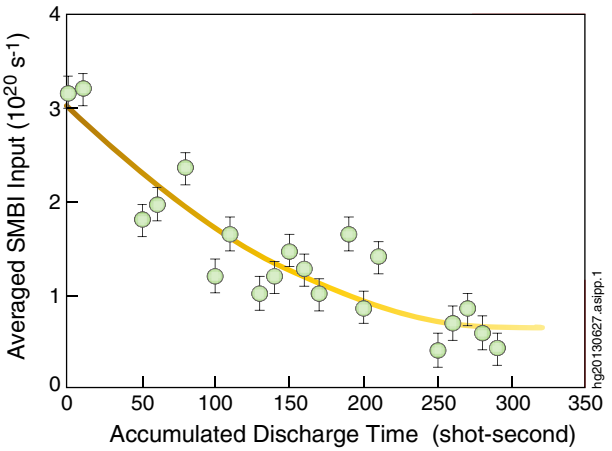

Figure 4. Averaged SMBI input required to maintain the same plasma density versus accumulated discharge time, following fresh Li coating.

($\leqslant 3\%$), which is essential for effective ICRF heating in the hydrogen minority heating scheme and promotes access to H-modes. Furthermore, we have carried out real-time Li gettering with the injection of fine Li powder at a flow rate of 30–50 mg s^{-1}, developed by the Princeton Plasma Physics Laboratory (PPPL) [13]. This enabled the achievement of the longest H-mode plasma in EAST during the 2010 experimental campaign, as shown in figure 2, in which Li powder was injected through the upper divertor gap.

Dedicated experiments have been carried out in EAST to assess Li pumping persistence. SMBI was used for precise density feedback control and modulating the gas fuelling with a well-defined SMBI pulse period to measure particle pump-out times in L-mode plasmas heated with lower hybrid waves. Divertor Langmuir probe data were also taken to measure ion saturation current response to the gas fuelling. The saturation current decay trends (related to local divertor recycling rates) were found to be consistent with the global pumping trends, as indicated by the total SMBI fuelling required to maintain a constant line-averaged electron density. The global density and local/divertor pump-out measurements were obtained for a variety of configurations including USN, DN and LSN, and up–down asymmetries in global pumping rates were evident.

Figure 3 shows the integrated SMBI particle input for four discharges following Li coating with similar plasma densities. As can be seen, the SMBI fuelling required to maintain the requested density decreases by nearly 30% within six shots as evident from comparing the two USN plasmas. Note that in order to assess Li pumping, the strike points were placed away from the entrance duct of the divertor cryopump, which is situated underneath the bottom divertor, to minimize the pumping effect from the cryopump. Hence, the required SMBI fuelling is nearly the same for both USN and LSN to maintain the same plasma density, as shown in figure 3. More data are shown in figure 4 for a series of discharges that followed the fresh Li coating, with each having a discharge duration of 10 s. In spite of the scatter due to the variation of operation conditions, the averaged SMBI input, i.e. the ratio of the total integrated particles from SMBI during each discharge to the discharge duration, exhibits a clear decreasing trend with the accumulated discharge time, and the result implies the degradation of strong pumping by Li after ~100 shot-seconds.

The density modulation produced by SMBI provides a convenient tool for evaluating the dynamics of particle recycling. A simple model was introduced to further quantify the effects of Li coating based on the divertor response to SMBI. During SMBI, a particle source term is introduced into the scrape-off layer (SOL). Since the particle loss rate is dominated by the parallel flow along the open field lines

connected to the divertor target with respect to the cross-field diffusion, the particle balance in a flux tube can be simply described as follows:

$$V\frac{\mathrm{d}n}{\mathrm{d}t} = S_0 + (\Gamma_{\mathrm{in}} - \Gamma_{\mathrm{out}})A \tag{1}$$

where V is the volume of the flux tube, n is the density, Γ_{in} and Γ_{out} represent the fluxes entering and exiting the flux tube with the area A, and S_0 is the source from SMBI. The influx, Γ_{in}, is due to recycling, i.e.

$$\Gamma_{\mathrm{in}} = R_{\mathrm{c}}\Gamma_{\mathrm{out}} \tag{2}$$

where R_{c} is the particle recycling coefficient. The out-flux, Γ_{out}, is regularly measured by the Langmuir probes and is directly proportional to the local density in the divertor. For a simple sheath-limited plasma regime Γ_{out} is given by [14]

$$\Gamma_{\mathrm{out}} = \tfrac{1}{2}nc_{\mathrm{s}} \tag{3}$$

where $c_{\mathrm{s}} = \sqrt{k(T_{\mathrm{e}} + T_{\mathrm{i}})/m_{\mathrm{i}}}$ is the ion sound speed. When the source from SMBI is turned off, i.e. $S_0 = 0$, the density decays as

$$n = n_0 \exp(-t/\tau) \tag{4}$$

with

$$\tau = \frac{2L_{\mathrm{c}}}{(1 - R_{\mathrm{c}})c_{\mathrm{s}}} \tag{5}$$

and

$$L_{\mathrm{c}} = 2\pi Rq \tag{6}$$

where R is the major radius, q is the edge safety factor, which is usually taken at the 95% flux surface.

The role of recycling should be reflected, therefore, in the characteristic decay time of the ion saturation current I_{s} (proportional to n), as measured by the Langmuir probes at the divertor target. Figure 5 shows the exponential fit applied to I_{s} (red curve) from a divertor Langmuir probe for each of the periods of time following SMBI pulses and corresponding decay times for a typical discharge. It appears that Li pumping gradually degrades during the discharge. Hence, the particle decaying time increases slightly at the beginning of the discharge, then saturates around 2.5 s, with $\tau \sim 25$ ms, for the case shown in figure 5. Note that the error bars are rather small, actually hidden beneath the symbols in the figure; the data scatter largely reflects the change in plasma conditions during the discharge.

One can see from equation (5) that as R_{c} approaches unity, the characteristic time increases to infinity. Alternatively, as R_{c} approaches 0, then the decay time reduces to the characteristic ion transit time of the flux tube, i.e. $\tau = 2L_{\mathrm{c}}/c_{\mathrm{s}}$. For the discharge with fresh Li coating, i.e. shot 42351, $\tau \sim 25$ ms. Under this discharge condition, the safety factor at the 95% flux surface, $q = q_{95} \sim 5$ and $T_{\mathrm{e}} \sim 20$ eV, as obtained from the divertor Langmuir probes. Hence, we found $R_{\mathrm{c}} \sim 0.89$ with fresh Li coating, based on equations (5) and (6), assuming $T_{\mathrm{e}} = T_{\mathrm{i}}$. This is consistent with the previous findings from NSTX, which demonstrated a reduction in the recycling coefficient from ~0.98 to ~0.90 with fresh Li coating [15, 16].

In order to facilitate density maintenance for long-pulse operations, we have employed, for the first time, SMBI for the active feedback control of plasma density. The newly developed SMBI system, located at the outer midplane on the low-field side, produces a rapid travelling gas jet with the speed exceeding 1 km s^{-1} and the pulse length ranging from 2 to 20 ms. This, with a low wall recycling achieved by Li coating, allows fast and accurate feedback control of plasma density, with an error <5%. To demonstrate this, figure 6 shows the time evolution of an L-mode discharge, which was initially driven by LHCD, followed by the application of modulated ICRH. The density was first ramped up, then maintained at the programmed level by SMBI until the end of LHCD, despite significant changes in current drive and heating conditions. SMBI has also been successfully demonstrated in EAST for the active control of ELMs [17].

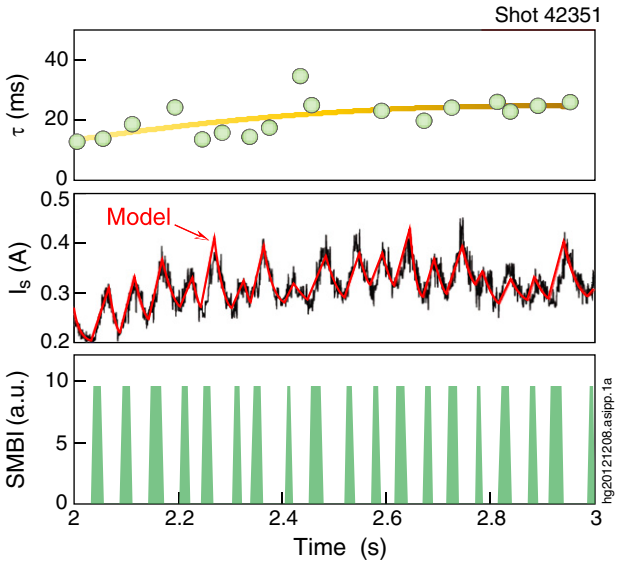

Figure 5. Decay time, τ, of divertor particle fluxes during SMBI pulses, as derived from the ion saturation current, I_{s}, obtained from a divertor Langmuir probe. SMBI waveform shown in green. I_{s} shown in black. Fitted model to data shown in red.

3. Effects of divertor configuration

3.1. H-mode access

The first H-mode was achieved in EAST in the experimental campaign in 2010, right after the 23rd IAEA Fusion Energy Conference, with predominantly LHCD [18]. The heating power available from LHCD was limited to ~1.3 MW at 2.45 GHz. To facilitate the access to H-modes, Li wall conditioning was routinely applied to reduce recycling and impurity radiation. Due to the limited heating power available, H-modes were obtained at marginal heating power with respect to the threshold power needed for the transition from L-mode to H-mode, achieving stationary H-modes with small ELMs up to 6.4 s with real-time Li injection (figure 2). In the recent 2012 campaign, such a small-ELM H-mode regime has been further extended with a record duration of 32 s, as shown in section 5.

The plasma shape and divertor configuration exhibit a significant influence on the access to H-modes [19–23]. However, the underlying physics mechanism is still unclear. Dedicated experiments were performed in the EAST 2012 Spring campaign to further investigate this. Figure 7 shows

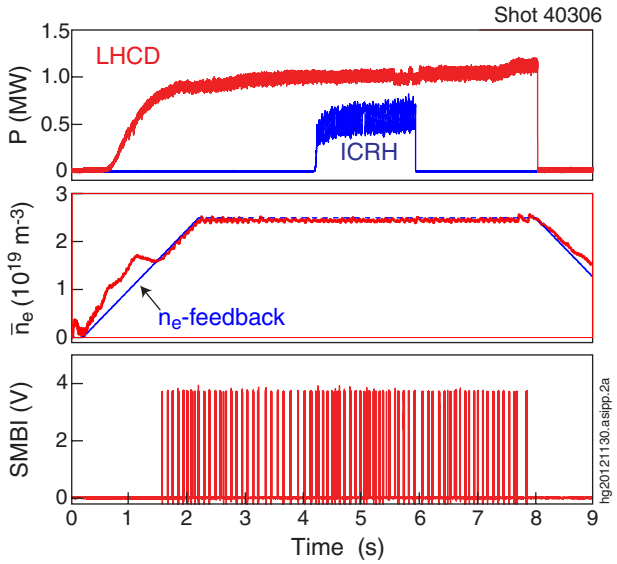

Figure 6. Demonstration of density feedback control by SMBI under fast varying current drive and heating conditions due to modulated ICRH. Time traces are shown for the auxiliary power from LHCD and ICRH, line-averaged density, $\bar{n}_e$, and SMBI waveform.

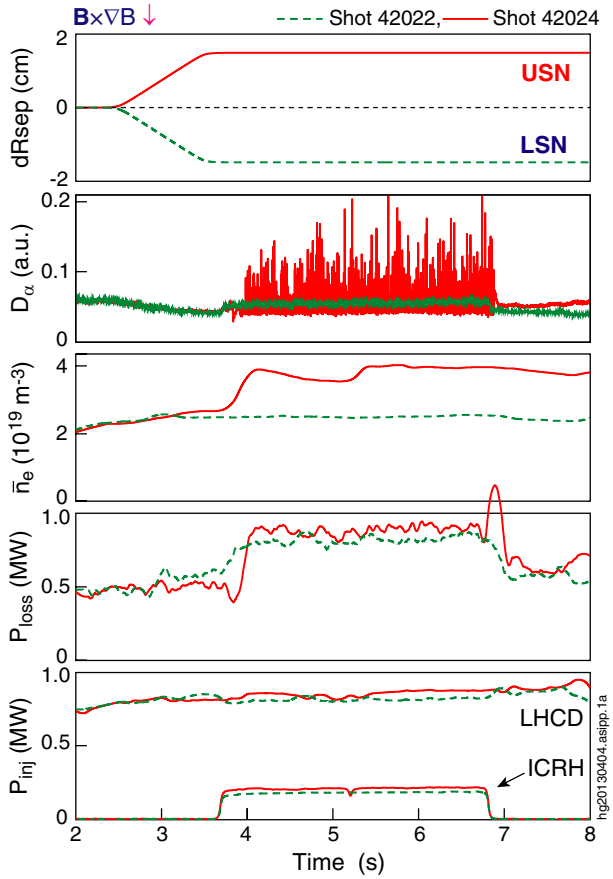

Figure 7. Comparison of L–H transition dynamics between LSN and USN for two discharges driven by LHCD with additional ICRH with similar initial operating conditions; $B_T = 2$ T (clockwise, viewing from top), $I_p = 0.4$ MA. H-mode only appears for USN, i.e. with the ion ∇B drift away from the active divertor, maintaining until the end of ICRH.

the effect of divertor configuration on the access to H-modes with LHCD and additional ICRH for USN and LSN for the ion ∇B drift direction towards the bottom divertor. The injected LHCD and ICRH power, P_{LHCD} and P_{ICRH}, are kept the same for the two different divertor configurations. The loss power across the separatrix, P_{loss}, is also similar for the two cases. $P_{\mathrm{loss}} = P_{\mathrm{OH}} + P_{\mathrm{LHCD}} + P_{\mathrm{ICRH}} - P_{\mathrm{rad}} - \mathrm{d}W_{\mathrm{dia}}/\mathrm{d}t$ is calculated as the sum of ohmic power, P_{OH}, absorbed auxiliary heating power from LHCD and ICRH, P_{LHCD} and P_{ICRH}, subtracting radiation, P_{rad}, and the time variation of the stored energy $\mathrm{d}W_{\mathrm{dia}}/\mathrm{d}t$. As can be seen, the H-mode is achieved and maintained with combined LHCD and ICRH under the USN divertor configuration with $\mathrm{d}R_{\mathrm{sep}} \sim 1.5$ cm (shot 42024)), as evidenced by the appearance of ELMs, as seen in the Balmer-alpha emission of deuterium, i.e. D_α. Here, $\mathrm{d}R_{\mathrm{sep}} = R_{\mathrm{sep\,L}} - R_{\mathrm{sep\,U}}$, with $R_{\mathrm{sep\,L}}$ and $R_{\mathrm{sep\,U}}$ being the lower and upper separatrix radii mapped to the outer midplane. In contrast, for LSN with $\mathrm{d}R_{\mathrm{sep}} \sim -1.5$ cm (shot 42022), the plasma remains in L-mode with a similar loss power to the USN case. The initial target plasma density is also similar in the two discharges. Hence, this suggests that the power needed for the L–H transition, P_{LH}, in EAST is lower with the ion ∇B drift away from the active divertor.

Note that previous results from DIII-D [19] and Alcator C-Mod [20] demonstrated a lower power threshold for L–H transition under LSN with the ion ∇B drift towards the active divertor. In contrast, the L–H transition exhibited a similar or lower H-mode threshold with the ion ∇B drift away from the active divertor in JET [22]; however, the H-mode confinement was compromised in this case, possibly arising from fast particle losses, as both B_T and I_p directions were changed, thus with counter neutral beam injection, to maintain edge helicity. This is what made the JET results less interesting for ITER, but the cause for this remains elusive. On the other hand, results from ASDEX-Upgrade and MAST [21] and more recent studies on NSTX [23] showed a minimum P_{LH} near balanced DN with $\mathrm{d}R_{\mathrm{sep}} \sim 0$. This strongly suggests that some key ingredients, e.g. neutral recycling, divertor geometry, etc, are still missing for the understanding of L–H transition. EAST exhibits a number of unique features that do not exist in other experiments, which may also play a significant role on the L–H transition, such as (1) extensive Li wall conditioning, which was observed to facilitate H-mode access by lowering the power threshold for the L–H transition [18]; (2) dominant LHCD, which was recently found to impose a profound change in the edge magnetic topology in EAST [24].

3.2. Divertor asymmetry during ELMs

The basic asymmetry in power and particle deposition for various divertor configurations was assessed in EAST for ohmic and L-mode plasmas [5, 25]. The in–out divertor asymmetry was exacerbated during the ELMs in H-modes, favouring the outer divertor [26]. It has recently been found that the divertor also exhibits an up–down asymmetry in the presence of ELMs. What is even more interesting is that such an up–down asymmetry appears to be sensitive to the ion ∇B direction. Figure 8 shows the contours of the ion saturation current density measured by the Langmuir probes, j_s, at the upper outer (UO) and lower outer (LO) divertor targets, along

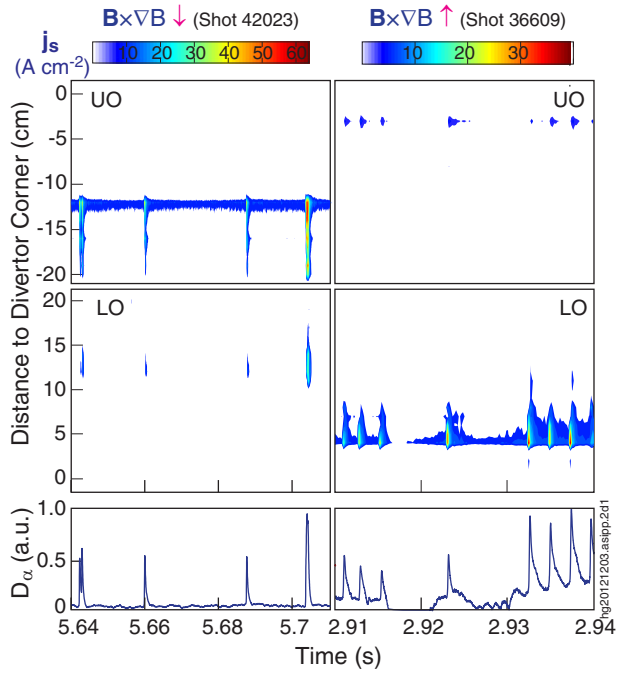

Figure 8. Contours of j_s at the UO and LO divertor targets for two ELMy H-mode discharges obtained under the DN divertor configuration, with the ion ∇B drift towards the bottom ($\boldsymbol{B} \times \nabla B \downarrow$) and top ($\boldsymbol{B} \times \nabla B \uparrow$) divertors, respectively. The time traces of D_α for the two discharges are also shown to identify the onset of ELMs.

with the time traces of D_α, for two ELMy H-mode discharges obtained under the DN divertor configuration with the ion ∇B drift towards and away from the active divertor, respectively. As can be seen, with the ion ∇B drift towards the bottom divertor ($\boldsymbol{B} \times \nabla B \downarrow$), more particle fluxes from ELMs go to the upper divertor target, i.e. in the *opposite* direction to the ion ∇B drift, as indicated by the contours of ion saturation current density, j_s. This trend is completely reversed as the ion ∇B drift direction is reversed, i.e. towards the top divertor ($\boldsymbol{B} \times \nabla B \uparrow$), with most of the particle fluxes reaching the bottom divertor target.

This is most likely due to classical drifts, as such an up–down asymmetry does not involve geometric effects. Recent modelling by Rozhansky *et al* using the SOLPS 5.2 transport code [27] shows that the up–down asymmetry is predominantly caused by the poloidal $\boldsymbol{E} \times \boldsymbol{B}$ drift, which is in the same direction as the ion ∇B drift in the SOL with $\boldsymbol{E}$ directed away from the separatrix. In the presence of drifts, the parallel particle flux should adjust accordingly to satisfy the boundary condition at the divertor target [27]:

$$V_{\mathrm{p}}^{E\times B} + b_{\mathrm{p}} V_{\parallel} = b_{\mathrm{p}} c_{\mathrm{s}}, \tag{7}$$

where $V_{\mathrm{p}}^{E\times B}$ is the poloidal flow associated with the $\boldsymbol{E} \times \boldsymbol{B}$ drift, which is of the same order as the poloidal ion sound speed, $b_{\mathrm{p}} c_{\mathrm{s}}$, and $b_{\mathrm{p}} V_{\parallel}$ represents the poloidal contribution from the plasma flow along the field lines. Hence, when the poloidal $\boldsymbol{E} \times \boldsymbol{B}$ drift (in the same direction as the ion ∇B drift) is directed towards the bottom divertor, the total ion fluxes are reduced at the bottom divertor target (LO). In contrast, when the $\boldsymbol{E} \times \boldsymbol{B}$ drift is directed towards the top divertor, most particle fluxes go to the bottom divertor, as observed by the divertor Langmuir probes (figure 8).

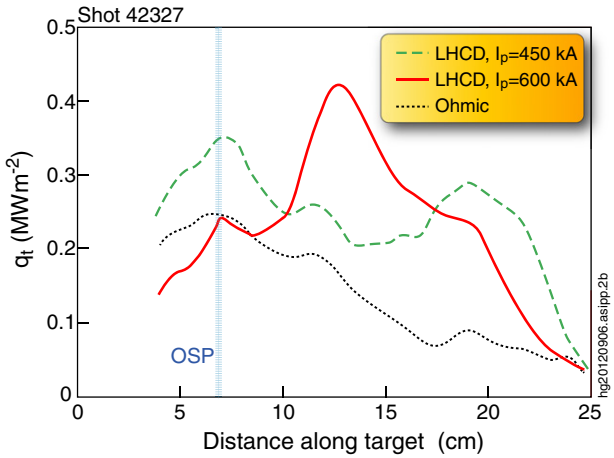

Figure 9. Comparison of heat flux profiles at the outer divertor target with and without LHCD at different plasma currents.

It is interesting to note that the operation with the ion ∇B drift towards the top divertor enhances the particle flow towards the bottom divertor, thus facilitating particle exhaust because the divertor cryopump is located at the bottom in EAST. Actually, this is indeed currently the preferred operating scenario on EAST.

4. Active control of target heat load

4.1. SHF induced by LHCD and effects of SMBI

It has been newly found on EAST that LHCD can induce a profound change in the magnetic topology by driving helical current filaments (HCFs) on the magnetic field lines in the divertor SOL [24]. The HCFs induce a 3D distortion of the edge magnetic field lines, similar to the resonant magnetic perturbations (RMPs). This leads to the splitting of divertor strike points, producing the SHF on the divertor target plate.

Figure 9 compares the heat flux profiles at the outboard divertor target plate with and without LHCD. As can be seen, with LHCD, the heat flux spreads over a large area on the divertor target plate, up to 20 cm away from the separatrix, exhibiting a multi-peak SHF structure. Note that the LHCD-induced SHF structure is affected by the plasma current. Increasing the plasma current reduces the distance between SHF and the outer strike point (OSP).

The degree of LHCD-induced SHF can be affected by SMBI. The application of SMBI reduces the peak heat flux near the strike point, while further enhancing the SHF in the far-SOL region. The amount of heat transferred from the OSP to the SHF increases with the SMBI pulse length, as shown in figure 10. The data were taken during a discharge, predominantly driven by LHCD, with the SMBI pulse length being varied from 8 to 12 ms. More details can be found in [17]. It appears, therefore, that SMBI, along with LHCD, provides a new tool for the control of divertor heat flux distribution for long-pulse operations.

4.2. Radiative divertor with Ar injection

The radiative divertor with impurity seeding provides an effective tool to reduce the peak heat load on the divertor target,

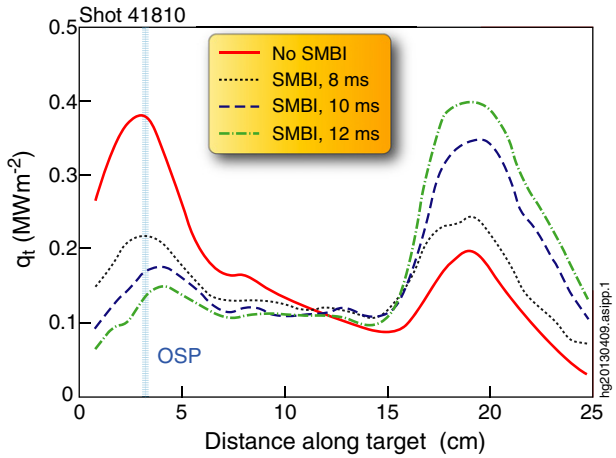

Figure 10. Profiles of target heat flux along the LO divertor target with and without SMBI for an LHCD-driven discharge with various SMBI pulse lengths, i.e. 8, 10 and 12 ms.

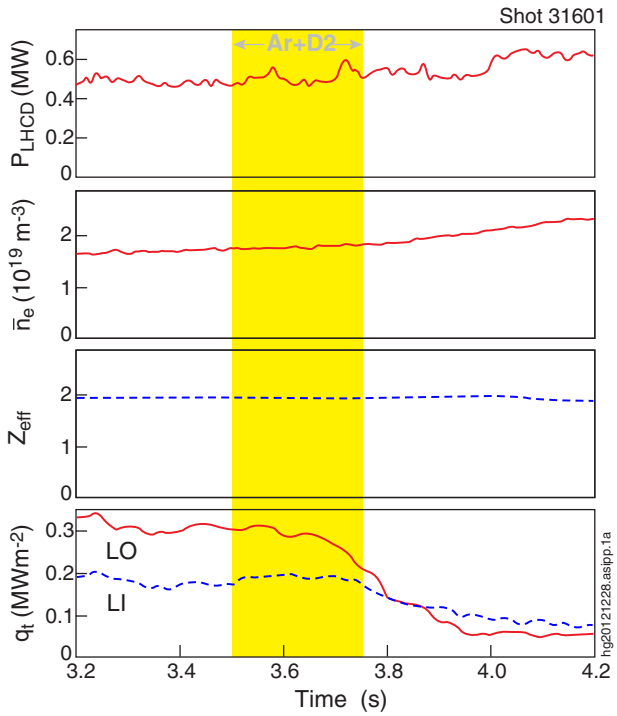

Figure 11. Time traces of injected LHCD power, P_{LHCD}, line-averaged density $\bar{n}_e$, Z_{eff} and heat flux q_t near the lower inner (LI) and outer (LO) strike points, showing the effect of Ar (25%) : D_2 puffing starting at ~3.6 s.

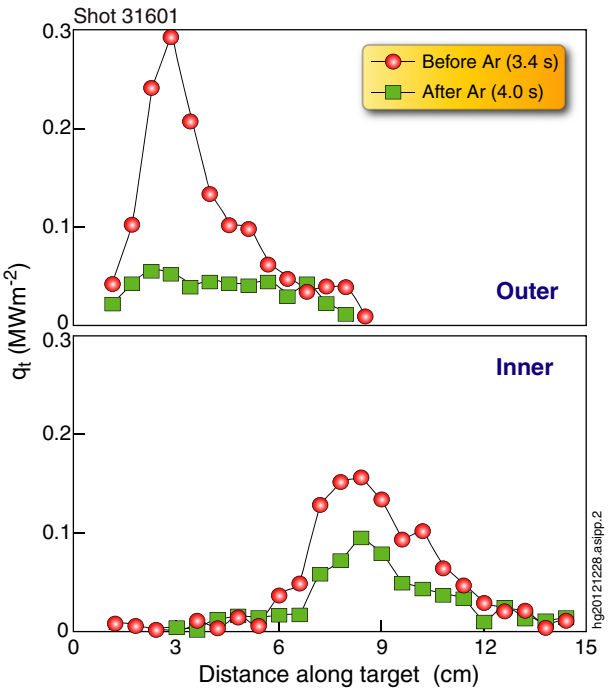

Figure 12. Heat flux profiles at the bottom inner and outer divertor targets versus distance to the respective divertor corner, obtained from the IR system, before and after the Ar puffing.

which is essential for long-pulse high-power operations [7, 28]. N_2 has been widely used in the present experiments because it has similar properties to the well-studied intrinsic carbon impurity in fusion experiments [28]. However, N_2 is not suitable for application in EAST, which heavily relies on Li wall conditioning, because N_2 can readily react with Li under normal conditions to form lithium nitride (Li_3N), passivating the Li coating. We have started to explore the radiative divertor scenarios, which are compatible with Li wall conditioning and core plasma performance, as an essential element of the EAST overall programme for achieving long-pulse high-power operations. Hence, efforts have been made on EAST using Ar as a seeded impurity to produce radiative divertor plasmas [29].

Localized divertor gas puffing with the D_2 : Ar mixture has been carried out in EAST to preferentially reduce peak heat fluxes near the OSPs, which are subject to the most intensive plasma impact. Figure 11 shows the time evolution of an L-mode discharge under the DN divertor configuration with the ion ∇B drift towards the top and the divertor cryopump being activated, $P_{LHCD} = 0.5$ MW, $I_p = 0.4$ MA, $\bar{n}_e \approx 1.7 \times 10^{19}$ m^{-3}. Ar is introduced into both top and bottom outboard divertors near the OSP at 3.5 s. However, the effect of Ar only starts to appear at about 3.7 s, mainly limited by the conductance of the gas pipeline. As expected, the heat flux, q_t, at the outer divertor target, obtained from an infrared (IR) camera, is dramatically reduced, i.e. by ~6 times, following the injection of an Ar : D_2 gas mixture (with 25% of Ar in D_2). The degree of heat flux reduction is much less pronounced at the inner divertor target, indicating small leakage of Ar from the outer to the inner divertor, thus mitigating the in–out divertor asymmetry. Despite Ar injection, Z_{eff} in the core plasma is little affected, suggesting strong divertor screening. Figure 12 compares the heat flux profiles before and after the Ar puffing. Clearly, the heat fluxes across the entire outer target are reduced after Ar puffing to the level even below that at the inner divertor target.

5. Progress on long-pulse divertor operations

Long-pulse L-mode diverted plasmas up to 411 s have been achieved with LHCD by carefully controlling the neutral recycling and heat load on the divertor targets. Figure 13 shows the time evolution of a typical long-pulse discharge, achieved with extensive Li wall coating, active water cooling and divertor cryopumping. In addition, the divertor configuration

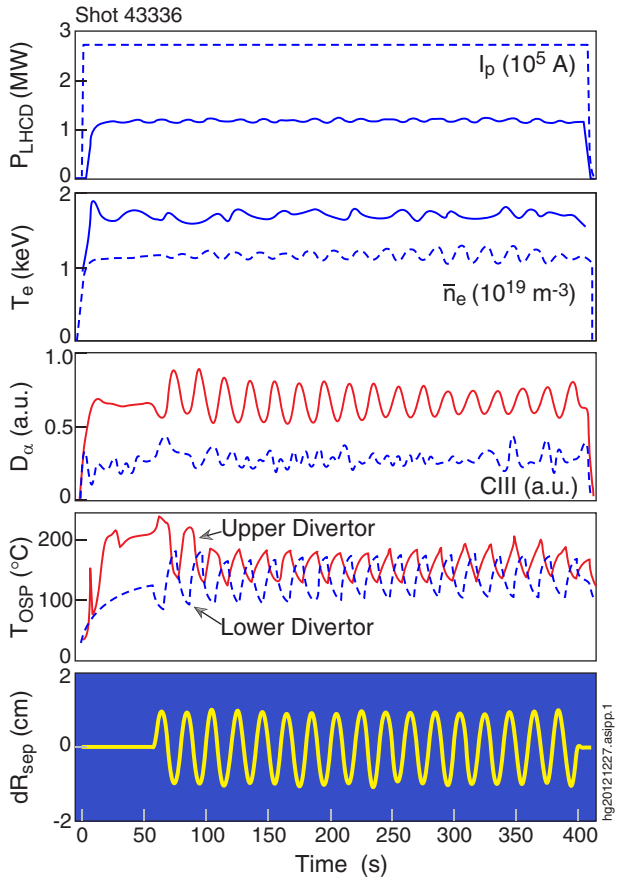

Figure 13. Time evolution of a long-pulse discharge over 400 s, entirely driven by LHCD, with the divertor configuration varying between LSN ($dR_{sep} < 0$), DN ($dR_{sep} = 0$) and USN ($dR_{sep} > 0$) during the discharge to spread heat loads. Temperatures at the OSP from the IR camera, T_{OSP}, also shown for both upper and lower divertors; $I_p \sim 270$ kA, $B_T \sim 2.5$ T.

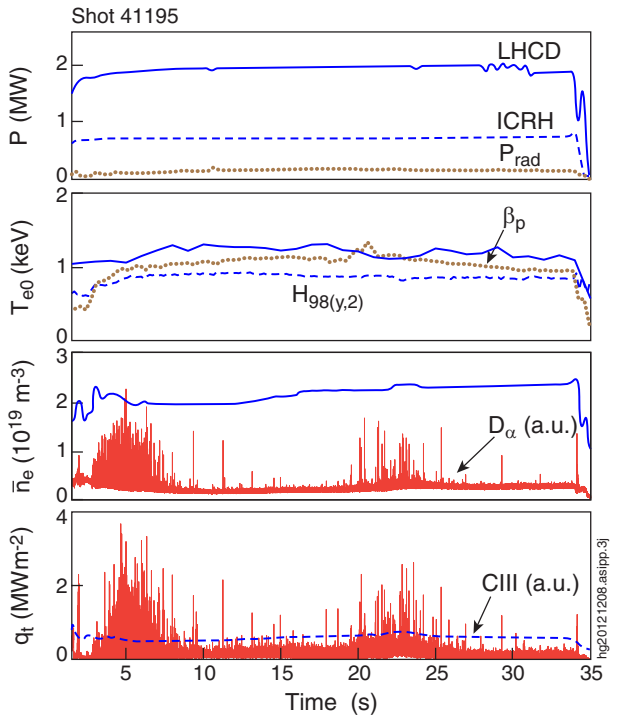

Figure 14. Time traces of an H-mode discharge over 30 s with $I_p \sim 0.28$ MA, $B_T = 1.9$ T, $n_e/n_G \sim 0.5$, achieved with combined LHCD and ICRH, including H-mode confinement factor $H_{98(y,2)}$, poloidal beta, β_p, central electron temperature, T_{e0}, heat flux, q_t, derived from divertor Langmuir probes.

was varied periodically from USN ($dR_{sep} > 0$) via DN ($dR_{sep} = 0$) to LSN ($dR_{sep} < 0$) during the discharge to spread heat loads and reduce the peak heat fluxes on the divertor targets. Real-time plasma control was also applied to maintain plasma shape to ensure effective coupling for LHCD. As can be seen, the temperatures at both upper and lower divertor targets are maintained below 200 °C throughout the discharge. Impurity influxes and neural recycling are also well controlled during the discharge, as indicated by C III (the line emission of C^{2+} ions) and D_α emissions. The discharge terminates normally, as programmed.

Reproducible, long-pulse H-modes have also been achieved in EAST with predominantly LHCD and extensive Li wall coating. The H-mode duration has now been extended over 30 s from 6.4 s in 2010, much longer than several tens of the current diffusion time, thus setting a record for the longest H-mode duration achieved to date. Figure 14 shows the time traces of a typical long-pulse H-mode driven by LHCD with additional ICRH, under the DN divertor configuration with the ion ∇B drift towards the top, $B_T \sim 1.9$ T, $I_p \sim 280$ kA, triangularity $\delta \sim 0.5$, elongation $\kappa \sim 1.7$, $q_{95} \sim 6.8$, normalized Greenwald density $n_e/n_G \sim 0.5$. This long-pulse H-mode regime exhibits a confinement quality between type-I and type-III ELMy H-modes, with the confinement factor, $H_{98(y,2)} \sim 0.9$, similar to the type-II ELMy H-mode [30]. The peak heat flux is largely below 2 MW m^{-2}, as determined from the divertor probe measurements.

6. Summary and future plans

Significant progress has been made on EAST towards long-pulse divertor operations on both technology and physics fronts, achieving long-pulse divertor plasmas up to 411 s, entirely driven by LHCD, and reproducible H-mode plasmas well over 30 s with predominantly LHCD, assisted by additional ICRH. To accomplish this, great efforts have been made to control divertor heat fluxes and edge recycling by improving PFCs with active water cooling and developing effective wall conditioning techniques. Li wall conditioning has proven to be the most effective method employed in EAST to control hydrogenic recycling, lowering the recycling coefficient down to $R_c \sim 0.9$ with fresh Li coating. In addition, real-time injection of Li powder has been demonstrated in EAST, which offers an attractive real-time wall conditioning technique for long-pulse plasma operations.

Contrary to expectations, access to H-modes in EAST exhibits a lower power threshold with the ion ∇B drift away from the active divertor. More investigations will be made in EAST during the next experimental campaign to explore the H-mode threshold over a wide range of plasma parameters for the different divertor configurations. In particular, since P_{LH} exhibits a minimum as a function of n_e, e.g. see [22], it is unclear how P_{LH} varies at or below the low-density threshold. Furthermore, the H-mode confinement quality will also be

examined for the scenarios with the ion ∇B drift away from or towards the active divertor. ELM particle fluxes also appear to be affected by the drifts, as evidenced by the dependence of the up–down asymmetry on the toroidal field direction for DN divertor configuration, with preferential particle flow in the direction opposite to the ion ∇B or $\boldsymbol{E} \times \boldsymbol{B}$ drift. Therefore, with the divertor cryopump located at the bottom in EAST, the operation with the ion ∇B drift towards the top divertor facilitates particle exhaust, which is currently the preferred operation scenario in EAST. Another new finding is that LHCD produces the SHF on the divertor targets, enhancing heat deposition away from the outer strike point, and the degree of SHF can be affected by changing the edge plasma conditions, i.e. by SMBI. In addition, Ar injection has been explored in EAST for the control of divertor heat fluxes.

The long-pulse H-mode achieved in EAST exhibits a confinement quality between type-I and type-III ELMy H-modes, with $H_{98(y,2)} \sim 0.9$, and peak heat fluxes largely below $2\,\mathrm{MW\,m^{-2}}$. This newly achieved H-mode scenario, enabled by Li coating and LHCD, may offer a promising option for long-pulse high-performance plasmas.

EAST is now undertaking an extensive upgrade with enhanced current drive and heating capabilities. To facilitate long-pulse, high-power operations, the upper divertor will be upgraded to the ITER-like W monoblock target structure with flat-type domes by the end of 2013, to allow for high heat load on divertor targets up to $10\,\mathrm{MW\,m^{-2}}$. The second in-vessel cryopump will be installed behind the outer target in the upper divertor to improve particle exhaust. In addition, an RMP system with two (poloidal) $\times$ eight (toroidal) coils is under construction, and will be available in the next campaign, together with many new or upgraded diagnostics. These will enable EAST to address some critical issues for long-pulse operations under ITER-relevant conditions in the near future.

Acknowledgments

This work was supported in part by the National Magnetic Confinement Fusion Science Program of China under Contracts Nos 2010GB104001, 2010GB104002, 2011GB101000, 2011GB107001, 2012GB101001 and 2013GB107003, the JSPS-NRF-NSFC A3 Foresight Program in the field of Plasma Physics (NSFC No 11261140328), as well as the Thousand Talent Plan of China. The views and opinions expressed herein do not necessarily reflect those of the ITER Organization.

References

[1] Wan Y.X. *et al* 2000 *Nucl. Fusion* **40** 1057
[2] Wan B. 2009 *Nucl. Fusion* **49** 104011
[3] Li J. and Wan B. 2011 *Nucl. Fusion* **51** 094007
[4] Guo H.Y. *et al* 2011 *J. Nucl. Mater.* **415** S369
[5] Guo H.Y. *et al* 2013 *J. Nucl. Mater.* **438** (Suppl.) S280
[6] Tsitrone E. 2007 *J. Nucl. Mater.* **363–365** 12
[7] Loarte A. *et al* 2007 Progress in the ITER Physics Basis: chapter 4. Power and particle control *Nucl. Fusion* **47** S203
[8] Xiao B.J. *et al* 2008 *Fusion Eng. Des.* **83** 181
[9] Yao L. *et al* 2001 *Nucl. Fusion* **41** 817
[10] Wan B. *et al* 2013 *Nucl. Fusion* **53** 104008
[11] Zuo G.Z. *et al* 2012 *Plasma Phys. Control. Fusion* **54** 015014
[12] Zuo G.Z. *et al* 2013 *J. Nucl. Mater.* **438** S90
[13] Mansfield D.K. *et al* 2010 *Fusion Eng. Des.* **85** 890
[14] Stangeby P.C. 2000 *The Plasma Boundary of Magnetic Fusion Devices* (Bristol: Institute of Physics Publishing)
[15] Canik J.M. *et al* 2011 *Phys. Plasmas* **18** 056118
[16] Maingi R. *et al* 2012 *Nucl. Fusion* **52** 083001
[17] Zou X.L. *et al* 2012 Divertor power deposition control and ELM mitigation with supersonic molecular beam injection in the EAST tokamak *24th IAEA Fusion Energy Conf. (FEC 2012) (San Diego, CA, 2012)* PD/P8-08, www-naweb.iaea.org/napc/physics/FEC/FEC2012/papers/792_PDP808.pdf
[18] Xu G.S. *et al* 2011 *Nucl. Fusion* **51** 072001
[19] Carlstrom T.N. *et al* 2002 *Plasma Phys. Control. Fusion* **44** A333
[20] Hughes J.W. *et al* 2007 *Fusion Sci. Technol.* **51** 317
[21] Meyer H. *et al* 2006 *Nucl. Fusion* **46** 64
[22] McDonald D.C. *et al* 2008 *Fusion Sci. Technol.* **53** 891
[23] Maingi R. *et al* 2010 *Nucl. Fusion* **50** 064010
[24] Liang Y.F. *et al* 2013 *Phys. Rev. Lett.* **110** 235002
[25] Liu S.C. *et al* 2012 *Phys. Plasmas* **19** 042505
[26] Wang L. *et al* 2012 *Nucl. Fusion* **52** 063024
[27] Rozhansky V. *et al* 2012 *Nucl. Fusion* **52** 103017
[28] Kallenbach A. *et al* 2011 *J. Nucl. Mater.* **415** S19
[29] Wang D.S. *et al* 2011 *Phys. Plasmas* **18** 032505
[30] Doyle E.J. *et al* 2007 Progress in the ITER Physics Basis: chapter 2. Plasma confinement and transport 2007 *Nucl. Fusion* **47** S18